Formation of a Copper Specific Binding Site in Non-Native States of β-2-Microglobulin†

Catherine M. Eakin, Jefferson D. Knight, Charles J. Morgan,‡ Michael A. Gelfand, and Andrew D. Miranker*

Department of Molecular Biophysics and Biochemistry, Yale University, 260 Whitney Avenue, New Haven, Connecticut 06520-8114

Received April 10, 2002; Revised Manuscript Received June 13, 2002

ABSTRACT: A debilitating complication of long-term hemodialysis is the deposition of β-2-microglobulin (β2m) as amyloid plaques in the joint space. We have recently shown that Cu^{2+} can be a contributing, if not causal, factor at concentrations encountered during dialysis therapy. The basis for this effect is destabilization and incorporation of β2m into amyloid fibers upon binding of Cu^{2+}. In this work, we demonstrate that while β2m binds Cu^{2+} specifically in the native state, it is binding of Cu^{2+} by non-native states of β2m which is responsible for destabilization. Mutagenesis of potential coordinating groups for Cu^{2+} shows that native state binding of Cu^{2+} is mediated by residues and structures that are different than those which bind in non-native states. An increased affinity for copper by non-native states compared to that of the native state gives rise to overall destabilization. Using mass spectrometry, NMR, and fluorescence techniques, we show that native state binding is localized to H31 and W60 and is highly specific for Cu^{2+} over Zn^{2+} and Ni^{2+}. Binding of Cu^{2+} in non-native states of β2m is mediated by residues H13, H51, and H84, but not H31. Although denatured β2m has characteristics of a globally unfolded state, it nevertheless demonstrates the following strong specificity of binding: $Cu^{2+} > Zn^{2+} \gg Ni^{2+}$. This requires the existence of a well-defined structure in the unfolded state of this protein. As Cu^{2+} effects are reported in many other amyloidoses, e.g., PrP, α-synuclein, and Aβ, our results may be extended to the emerging field of divalent ion-associated amyloidosis.

The conversion of normally soluble proteins into amyloid fiber is a common feature of a number of clinical disorders, including Alzheimer's, type II diabetes, and spongiform encephalopathies (*1*). Furthermore, many proteins which do not form pathogenic fibers, e.g., myoglobin, have nevertheless been shown to convert to amyloid under laboratory conditions (*2*). Amyloid fibers formed from different proteins have many features in common. They are unbranched, resist proteolytic digestion, and display green birefringence upon staining with the histological dye Congo Red. The tertiary and quaternary structure of amyloid fibers has been determined from X-ray diffraction studies to be cross-β, with the β-strands arranged orthogonal to the fiber axis and hydrogen bonding parallel to the fiber axis (*3*). The kinetics of amyloid formation include a lag phase suggesting nucleation-dependent kinetics akin to crystallization (*4*). The similarity of fiber formation kinetics to crystallization includes the ability to bypass the lag phase by providing exogenous seed. Interestingly, while amyloids from different proteins share common histological and ultrastructural features, seeded reaction kinetics are dependent on using the seed of the same or closely related protein sequence. This has been used, for example, to examine species barrier crossing in the yeast prion system (*5*). Thus, despite apparent histological and ultrastructural similarities, amyloid fiber must have specific atomic structures which mediate their assembly.

General determinants for amyloid formation have eluded identification; to date, only two structural features of polypeptides have been found to contribute. The first is a glutamine rich sequence such as that found in Huntingtin (*6*), and Sup35 from *Saccharomyces cerevisiae* prion (*7*). It is proposed that these sequences are stabilized by intersheet hydrogen bonding mediated by the glutamine side chains (*8*). The second is the presence of side chains which can interact with divalent metal, particularly Cu^{2+}. An increasing number of systems have been shown to display this property, including mammalian prion (*9*), Aβ from Alzheimer's (*10*), α-synuclein from Parkinson's (*11*), immunoglobulin light chains (*12*), and β2m from dialysis-related amyloidosis (*13*).

β2m is the 12 kDa polypeptide subunit that is necessary for the cell surface expression of the class I major histocompatibility complex (MHC)[1] (*14*). The turnover of MHC

† Supported by a grant from the National Institutes of Health (DK54899) and the Pew charitable trusts (PO219SC). A.D.M. is a Pew scholar in the biomedical sciences. C.M.E. receives support from an NIH training grant (5T32GM07223). J.D.K. is supported by a National Science Foundation Graduate Research Fellowship.

* To whom correspondence should be addressed. Phone: (203) 432-8954. Fax: (203) 432-5175. E-mail: Andrew.Miranker@yale.edu.

‡ Present address: Genzyme Corp., 1 Mountain Road, Framingham, MA 01701.

[1] Abbreviations: β2m, β-2-microglobulin; CD, circular dichroism spectroscopy; DRA, dialysis-related amyloidosis; ESI-MS, electrospray ionization mass spectrometry; MHC, major histocompatibility complex; NMR, nuclear magnetic resonance spectroscopy; NOESY, nuclear Overhauser effect spectroscopy; PAGE, polyacrylamide gel electrophoresis; SDS, sodium dodecyl sulfate; rWT, wild-type human β2m from *E. coli*, possessing an additional N-terminal methionine; hWT, human-derived β2m.

10.1021/bi025944a CCC: $22.00
Published on Web 08/03/2002

results in release of soluble β2m followed by catabolism by the kidney. For patients suffering from kidney disease treated by dialysis, β2m forms amyloid deposits principally in the joints, resulting in a variety of arthropathies. The circulating concentration of β2m in dialysis-related amyloidosis (DRA) patients can be 5−50 times the normal level of 0.1 μM. However, while elevated levels of protein are necessary for amyloid deposition, they are not sufficient. β2m concentrations do not correlate with the pathology of DRA (*15*), nor does β2m readily aggregate *in vitro* even at millimolar concentrations (pH 7) and salt concentrations isotonic with serum (*16*). We have recently shown that Cu^{2+} binds to β2m in a manner which is specific and at concentrations which can be encountered during dialysis therapy (*13*). Furthermore, the binding of Cu^{2+} by β2m results in destabilization and subsequent amyloid fiber formation. In this work, we have identified the residues responsible for binding and destabilization of the protein through the combined use of mutagenesis and analysis by native state mass spectrometry, NMR, and fluorescence.

MATERIALS AND METHODS

Chemicals. Buffers and salts obtained from either Sigma-Aldrich (Milwaukee, WI) or J. T. Baker (Phillipsburg, NJ). Cell culture media were purchased from Becton Dickinson (Sparks, MD).

Wild-Type and Mutant β2m Overexpression and Purification. β2m was expressed in *Escherichia coli* using plasmid pHN1, a gift from D. C. Wiley (Harvard University, Cambridge, MA). BL21(DE3) competent cells were transformed and grown in Luria broth in the presence of ampicillin (100 μg/mL). Cultures were grown at 37 °C to an OD at 600 nm of 0.6 and then induced with 500 μM IPTG for 2 h. Cells were harvested by centrifugation and lysed by sonication. Inclusion bodies were extracted, washed six times with 1 M urea, 100 mM Tris, 100 mM EDTA, and 10 mM methionine (pH 8.0), and resuspended in 8 M urea, 100 mM Tris, 100 mM EDTA, and 10 mM methionine (pH 8.0) for 24 h at 4 °C. Insoluble material was removed by centrifugation, and the soluble protein was refolded by dialysis against 25 mM potassium phosphate, 150 mM KCl, 1 mM EDTA (pH 7.4), and 10 mM methionine at 4 °C. After dialysis, the protein was concentrated by centrifugation using Vivascience (5 kDa cutoff) and run over a gel filtration column with Sephedex-75 resin at 4 °C and pH 7.4. The final purity was assessed by SDS−PAGE and electrospray ionization mass spectrometry (ESI-MS). Site specific mutations of β2m were made using Quickchange (Stratagene, La Jolla, CA) and sequenced (Keck facility, Yale University) to confirm the mutation. The mutant plasmids were purified as wild-type β2m and confirmed by SDS−PAGE and ESI-MS. Human-derived β2m was purified as previously described (*13*). Briefly, urine from Dent's disease patients (Yale School of Medicine Human Investigation Committee protocol 11522) was filtered (0.2 μm) and applied directly to a Cu^{2+}-charged NTA-Superflow column (Qiagen), washed (three times) with 5 mM KP (pH 7.4) and 150 mM KCl and five times with no salt and 1 mM imidazole. The protein was fractionated upon elution with 10 mM imidazole. β2m-containing fractions were pooled, concentrated, and further purified by size exclusion as performed for *E. coli*-derived β2m.

Determination of the Oxidation State. Oxidized and reduced wild-type and mutant β2m were analyzed by reverse-phase HPLC using a Vydac C18, 300 Å,4.6 mm × 250 mm column. Gradient separations were performed using an acetonitrile/water gradient (1%/min) in the presence of 0.1% trifluoroacetic acid, with a flow rate of 1 mL/min. Samples were denatured (6 M guanidinium chloride) in the presence or absence of freshly prepared dithiothreitol (∼1 mM) overnight prior to being applied to the column. The fraction of protein in the reduced state was determined from a comparison of the integrated peak area at elution times corresponding to fully oxidized or reduced β2m standards. The dynamic range of this approach permits us to confidently detect as little as 1% residual reduced protein in our samples.

Circular Dichroism (CD). CD experiments were performed on an Aviv model 215 spectrometer. Far-UV spectra (190−240 nm) were collected in a 1 mm path-length cell with 30 μM β2m in 25 mM potassium phosphate and 150 mM KCl (pH 7.4). Near-UV spectra (240−330 nm) of 100 μM β2m in the same buffer were recorded in a 3 mm path-length cuvette.

Fluorescence. Metal binding to the native state and the chemical stability of β2m were monitored by following changes in intrinsic fluorescence on a PTI Quantamaster C-61 with slit widths of 2 nm and excitation at 283 nm. In metal binding experiments, protein was diluted to 2.5 μM with a buffer containing the stated metal salt, 25 mM MOPS, and 150 mM potassium acetate at (pH 7.4). Chemical stability measurements were taken under the same buffer conditions over a range of urea concentrations. For chemical denaturation, samples were allowed to equilibrate for at least 12 h prior to data acquisition. Results are expressed as the average emission wavelength, $\langle\lambda\rangle$, calculated from the emission between 300 and 450 nm (*13*, *17*).

Mass Spectrometry. Spectra were acquired from 200 to 5000 *m*/*z* with signal averaging for 1 min using a Micromass LCT electrospray time-of-flight mass spectrometer. Atmospheric pressure ionization was performed using borosilicate glass capillaries drawn and sputter coated in-house. All mass determinations were made using a minimum of three charge states. External calibrations were performed with 20 mM CsI in H_2O ionized under matched instrument conditions. The temperature of the mass spectrometer ionization source was maintained at 20−25 °C. Protein ion counts of metal-bound and unbound forms of β2m were determined from the +7 charge state.

Calculations. Multiple-sequence alignment was performed using the mature human wild-type sequence as a query string to fasta33t (*18*) at www.ebi.ac.uk. Default parameters were used apart from limiting the upper expectation value to 10^{-10} which had the effect of restricting hits to alternative variants of β2m. Consensus analysis was performed using MView version 1.41.8 (*19*). Molecular graphics and solvent exposure calculations were performed using MolMol (*20*, *34*). The extent of solvent exposure was determined on residue side chains using a 1.4 Å probe radius. All curve fitting in this work was performed using the NonlinearRegress function in Mathematica 4.0 (Wolfram Research, Inc., Champaign, IL).

NMR. NMR spectra were recorded in house using a Varian Unity Plus instrument with proton resonance of 600 MHz. NOESY spectra were collected using a standard pulse

sequence with a mixing time of 200 ms. Two thousand points were collected in t_2, and 256 increments were collected in t_1. Data were processed using NMR PIPE (*21*) and analyzed using Sparky (*22*). The apo sample was 400 μM β2m, 0.4 mM d_{12}-EDTA, 10% D_2O, 150 mM KCl, and 25 mM potassium phosphate buffer at pH 7.0 and 37 °C. The holo sample was 500 μM β2m, 60 μM $CuCl_2$, 10% D_2O, 150 mM KCl, and 25 mM phosphate buffer at pH 7.0 and 37 °C. TMSP was included in both samples for reference.

RESULTS

In this work, we seek to delineate the role of divalent metal in native state binding and destabilization of β2m. The side chain ligand most likely to be involved in these interactions is histidine. Therefore, a series of four mutants have been prepared in which each histidine residue of β2m has been changed to a noncoordinating moiety. The affinity of a divalent ion for protein reflects both chemical and structural effects, the latter resulting from the three-dimensional orientation of the coordinating moieties of the protein. We have therefore made comparative measurements of β2m in the presence of Cu^{2+}, Zn^{2+}, and Ni^{2+}.

Native State Structure. The native state copper binding site was initially elucidated by a combination of ^{1}H NMR and intrinsic fluorescence. ^{1}H$-^1$H NOESY spectra of β2m acquired in the presence and absence of $CuCl_2$ indicate that H31 is involved in binding. The basis for this observation by NMR is the paramagnetic broadening of resonances near the binding site. To avoid complications from both nonspecific paramagnetic broadening and protein aggregation at high concentrations of protein and copper (*13*), substoichiometric (1:8) amounts of Cu^{2+} were used. Paramagnetic broadening resulted in the diminishment of peaks previously assigned (*16*) to the side chain of H31. For example, cross-peaks involving the C_ϵ proton of H31 (Figure 1A) are absent in spectra in which Cu^{2+} is present (Figure 1B). This is similar to previously reported ^{1}H$-^1$H TOCSY observations (*23*) in which H31 and also H13 resonances are affected by the presence of Cu^{2+}. Under our conditions, the cross-peaks of the C_ϵ proton are completely eliminated. As substoichiometric amounts of copper are being used, this indicates that chemical exchange of copper is rapid compared to the relaxation time.

The intrinsic fluorescence of β2m is principally derived from its two indole side chains, W95 and W60. The fluorescence emission of β2m in the presence of Cu^{2+} both decreases in intensity and shifts to shorter wavelengths (Figure 6 and ref *13*). At saturating levels of Cu^{2+}, the maximal decrease in intensity is ~40% and the blue shift is 6 nm. Since a buried indole is expected to emit at shorter wavelengths, these properties are consistent with a model in which a solvent accessible tryptophan is quenched by interaction with Cu^{2+}. W60 is more solvent exposed than W95 (75 vs 9%, respectively) (*24*), implying W60 is proximal to the Cu^{2+} binding site. Indeed, the crystal structure of β2m reveals that W60 and H31 are only ~7 Å apart (Figure 2B), further reinforcing the observation that H31 is part of the native state binding site.

The specificity for Cu^{2+} binding by the native state (*13*) suggests a physiological role for Cu^{2+} binding. This is supported by its multiple-sequence alignment analysis showing conservation of H31 across 87 sequence variants (Figure 2C). Of the four histidine residues in human β2m (Figure 2A), those at positions 31 and 84 are 100% conserved across species with as little as 37% total sequence identity. In contrast, those at positions 13 and 51 are more variable. This conservation correlates with the relative levels of solvent exposure of these residues; H13 and H51 are ~70% exposed (Table 1), while H31 and H84 are 38 and 0% exposed, respectively. Sequence conservation of H84 likely reflects a role in the packing of the protein core. In contrast, as residue H31 is not wholly buried, its conservation suggests a potential physiological role.

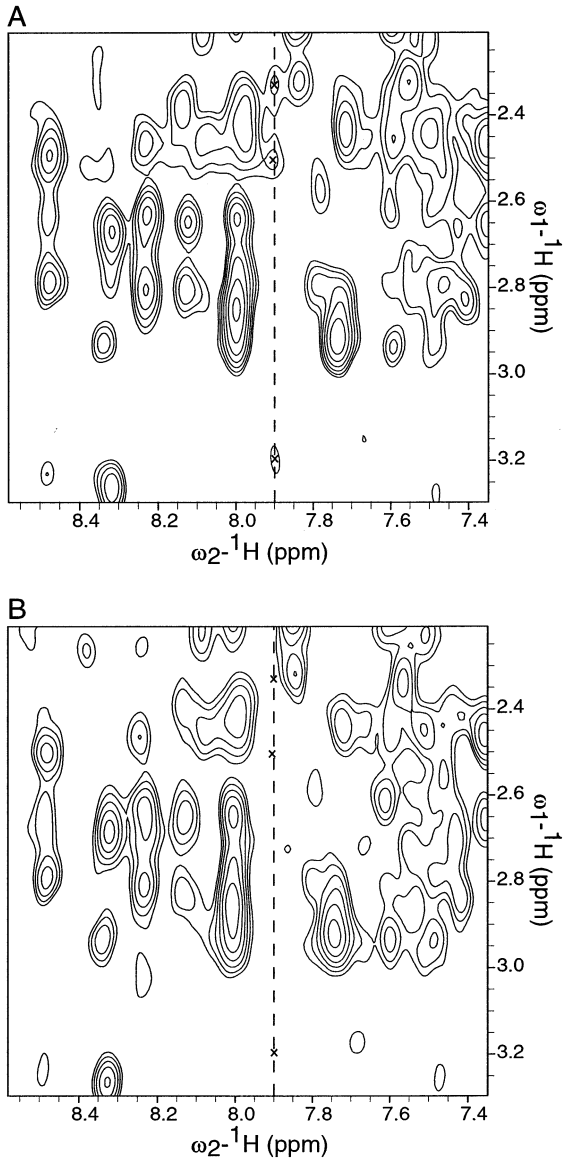

FIGURE 1: (A) ^{1}H$-^1$H NOESY spectrum of 400 μM β2m in the presence of 0.4 mM EDTA. (B) ^{1}H$-^1$H NOESY spectrum of 500 μM β2m in the presence of 60 μM $CuCl_2$. The dashed line at $\omega_2 = 7.9$ ppm corresponds to H31 Hϵ (*16*). A total of nine peaks (of which three are shown) were present at this resonance in the EDTA spectrum; all of these were absent or significantly less intense in the presence of copper. Spectra shown are contoured at the same level renormalized to the average of six invariant cross-peaks in the aromatic region of the spectra.

Mutant Protein Characterization. To identify the Cu^{2+} binding site and probe the role of Cu^{2+} binding and destabilization, each of the histidine residues in β2m (H13,

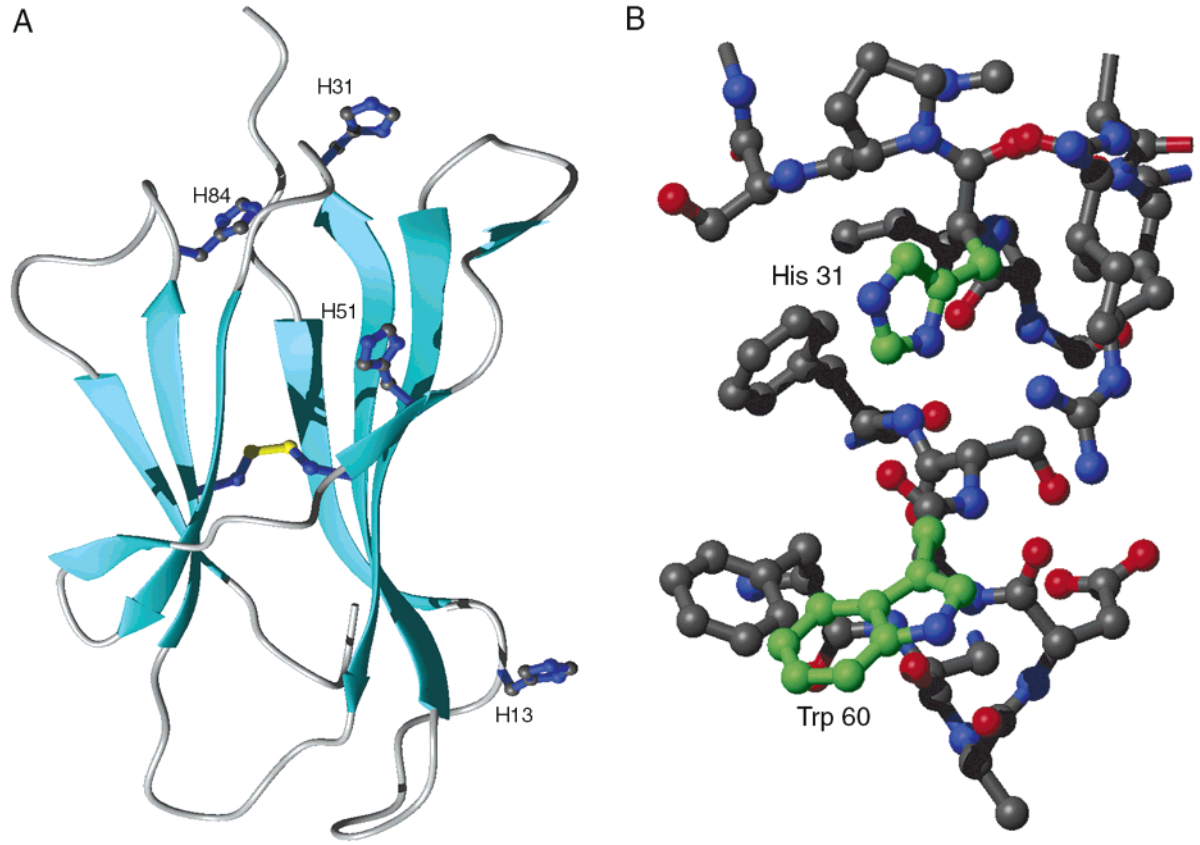

C

Species	Identity	Sequence
Human	100%	IQRTPKIQVYSRHPAENGKSNFLNCYVSGFHPSDIEVDLLKNGERIEKVEHSDLSFSKDWSFYLLYYTEFTPTEKDEYACRVNHVTLSQPKIVKWDRDM
Orangutan	96%	IQRTPKIQVYTRHPAENGKSNFLNCYVSGFHPSDIEVDLLKNGVKIEKVEHSDLSFSKDWSFYLLYYTEFTPTEKDEYACRVNHVTLSQPKTVKWDRDM
Mouse	70%	IQKTPQIQVYSRHPPENGKPNILNCYVTQFHPPHIEIQMLKNGKKIPKVEMSDMSFSKDWSFYILAHTEFTPTETDTYACRVKHDSMAEPKTVYWDRDM
Chicken	47%	ADLTPKVQVYSRFPASAGTKNVLNCFAAGFHPPKISITLMKDGVPMEGAQYSDMSFNDDWTFQRLVHADFTPSSGSTYACKVEHETLKEPQVYKWDPEF
Medaka Fish	37%	KTSPPTVQVYSRDPGQYGKENTLICHVSNFHPPDITIRLMEDDQELPEAKQTDLAFKQNWHFHLTKSAPFTPKQGARYTCKVTHSGLA--KDYTWESNM
Consensus	90%	...sPplQVYSR.Psp.Gc.NhL.CaVotFHPspIplphLKsG..h.tsp.oDLuFppsWpFalhh.stFTPspt-pYsC+VpH..h.t.p.h.W....

FIGURE 2: (A) Ribbon structure of β2m (2CLR) with histidine and cysteine residues shown with a ball-and-stick rendering. (B) Ball-and-stick rendering of atoms within 8.5 Å of the ϵ-carbon of H31. Carbon atoms of H31 and W60 are shown in green. (C) Summary of multiple-sequence analysis of 87 sequence variants of β2m. A selected subset are shown along with the consensus analysis for all 87 sequences.

Table 1: Summary of Measured Free Energies of Unfolding and Dissociation Constants for Cu^{2+}

	$\Delta G^{apo\ a}_{unfolding}$	$m_{apo}{}^a$	$\Delta G^{holo\ b}_{unfolding}$	$m_{holo}{}^b$	$K_d{}^c$	$\Delta G^{Cu\ d}_u$	$\Delta\Delta G^{Cu\ e}_u$	exposure^f
WT	33.0 ± 2.2	5.4 ± 0.4	12.0 ± 0.7	3.6 ± 0.2	2.8 ± 0.4	29.6	NA	NA
H13F	33.5 ± 3.4	5.0 ± 0.5	20.6 ± 0.7	3.7 ± 0.1	3.2 ± 0.4	21.2	8.4	70
H31F	43.9 ± 2.3	6.3 ± 0.3	17.0 ± 0.3	3.6 ± 0.2	41.0 ± 2.7	28.8	0.8	38
H51F	25.0 ± 0.3	4.0 ± 0.05	16.0 ± 0.9	3.4 ± 0.1	1.7 ± 0.3	18.9	10.7	67
H84A	22.0 ± 0.6	4.4 ± 0.1	14.0 ± 0.3	3.7 ± 0.06	1.5 ± 1.4	18.1	11.5	0

[a] Free energy and m values of unfolding in the absence of added metal (Figure 4). [b] Free energy and m values of unfolding in the presence of 90 μM $CuCl_2$ (Figure 4). [c] Dissociation constant for Cu^{2+} from β2m (Figure 6). [d] The calculated free energy of copper dissociating from the unfolded state at 90 μM Cu^{2+} (ΔG^{Cu}_f) based on the model discussed in the text ($\Delta G^{Cu}_u = \Delta G^{apo}_{unfolding} + \Delta G^{Cu}_f - \Delta G^{holo}_{unfolding}$) is determined using K_d in column 3. [e] Relative contribution of each histidine to the calculated free energy of copper binding to the unfolded state ($\Delta\Delta G^{Cu}_u$ = WTΔG^{Cu}_u − mutant ΔG^{Cu}_u). [f] Percent solvent exposure of the histidine side chain in 2CLR. Units of ΔG are kilojoules per mole. Units of m values are kilojoules per mole per molar. Units of K_d are micromolar.

H31, H51, and H84) was individually mutated to phenylalanine using standard methods. In the case of H84, mutation to Phe resulted in an unstructured protein (data not shown). This residue was therefore mutated to alanine. All constructs were purified by the same method used for the recombinant wild-type protein (rWT), producing H13F, H31F, H51F, and H84A β2m mutants. The purity was assessed by SDS−PAGE and mass spectrometry. Only bands attributed to β2m were visualized by SDS−PAGE, and masses determined by ESI-MS are within 0.1% of the calculated mass. The oxidation state of the C25−C80 disulfide in β2m was evaluated using a chromatographic approach (see Materials and Methods). Human-derived β2m, (hWT), H13F, H51F, and H84A did not exhibit any detectable reduced protein (data not shown). Recombinant WT (rWT) and H31F each have ~9% reduced protein. For the stability and ligand binding measurements performed here, rWT and hWT are indistinguishable, suggesting that these small amounts of reduced material are not significant in measurements of global properties.

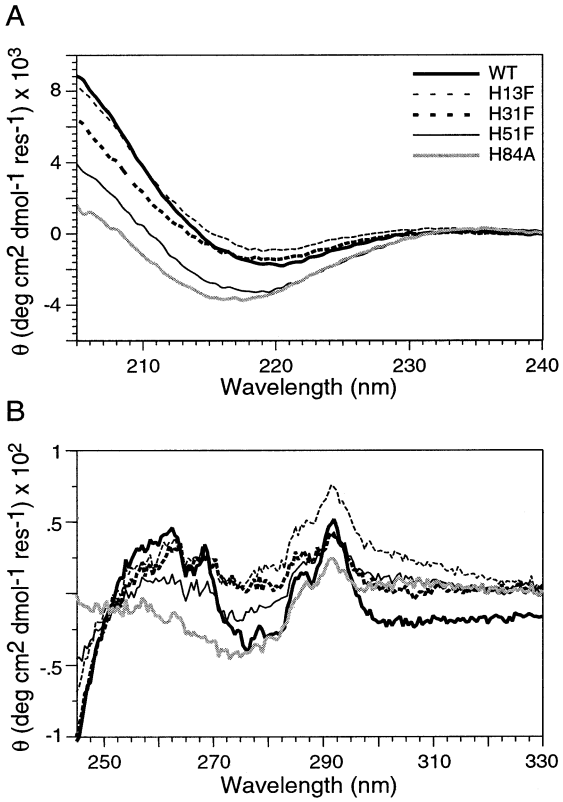

FIGURE 3: Far-UV (A) and near-UV (B) CD spectra of wild-type and mutant constructs of β2m. Near-identical profiles demonstrate that the global structures of wild-type and mutant β2m are identical. Small changes, particularly in the near-UV CD, are consistent with mutations occurring in aromatic regions of the polypeptide. WT spectra of the recombinant protein are shown.

All constructs used in this work are folded with secondary and tertiary structure consistent with the wild-type protein. Assessment of structure in rWT, H13F, H31F, H51F, and H84A β2m was performed using far- and near-UV CD. All demonstrate weak negative ellipticity (Figure 3A) at 220 nm, as is characteristic of a β-sheet fold (Figure 2A). H51F and H84A, however, have somewhat more negative ellipticity at 220 nm than rWT. This may be attributed to the breaking of one or more hydrogen bonds upon mutation of the histidine, resulting in small changes to the secondary structure. In the near-UV CD spectrum, positive bands were observed at 270 and 290 nm (pH 7.4) for the wild type, and all mutations. These bands arise from the packing of aromatic groups into a well-defined and fixed conformation (Figure 3B). Individual mutations in β2m vary only slightly compared to WT in near-UV CD, indicating that the mutants are both folded and have nearly identical atomic arrangements.

Wild-type and mutant constructs all show cooperative two-state transitions upon titration with urea (Figure 4), providing further evidence that the mutant proteins are folded. The stability (ΔG) and linear dependence of stability on urea concentration (*m* value) (*25*) of H13F are nearly identical to those of the wild type (Table 1). This is consistent with the fact that H13 is 70% solvent exposed, and does not participate in any intramolecular hydrogen bonding. Mutation of H84 and H51 results in destabilization of 11.0 and 8.0 kJ/mol, respectively, compared to WT. This is likely the result of lost hydrogen bonding and changes in solvent exposure. For example, the difference in buried surface area upon mutating H84 to Ala is ~80 Å^3, and two hydrogen bonds are lost (T86 and the backbone of S33) (*24*). In contrast, H31F displays a net stabilization of −10.9 kJ/mol. This suggests that the local structure around H31 is normally under strain.

Cu^{2+} Effects on Conformational Stability. The contribution of each histidine residue to Cu^{2+} induced destabilization was assessed by urea titration in the presence and absence of added Cu^{2+} (Figure 4). The most notable feature of this analysis is that destabilization by Cu^{2+} is enhanced rather than diminished in the H31F construct. Under near-physiological conditions (150 mM potassium acetate at pH 7.4 and 25 °C), WT β2m is destabilized 21.0 kJ/mol by the addition of 90 μM Cu^{2+} [Table 1 (33.0 − 12.0 kJ/mol) and Figure 4A,D]. In H31F, the protein is destabilized by 26.9kJ/mol upon addition of Cu^{2+} (Figure 4C,D). All other constructs have a reduced sensitivity to Cu^{2+}. H13F, H51F, and H84A are destabilized by 12.9, 9.0, and 8.0 kJ/mol, respectively. This reduced destabilization suggests that these three histidine residues are dominant in Cu^{2+} binding by non-native states of β2m. In contrast, the increased Cu^{2+} sensitivity of H31F compared to that of WT suggests that H31 interactions with Cu^{2+} are dominant in folded states of β2m.

The specificity of Cu^{2+} induced destabilization was assessed by urea titration of wild-type β2m in the presence of Ni^{2+} or Zn^{2+}. At 90 μM Ni^{2+} or Zn^{2+}, β2m is not destabilized (Figure 5A). Specificity was therefore determined using relatively high concentrations of Ni^{2+} and Zn^{2+} compared to the concentration of Cu^{2+}. At 20 μM Cu^{2+}, WT β2m is destabilized by 9.8 kJ/mol (Figure 5B). Addition of 400 μM Ni^{2+} to β2m resulted in no detectable change to the urea titration profile (data not shown). At 2000 μM Ni^{2+}, the urea titration profile has shifted, giving a midpoint of 6.6 M urea compared to a midpoint of 6.1 M urea for no divalent ion. The free energy of unfolding, however, is within error of metal free β2m (−30.6 kJ/mol). The analogous study with Zn^{2+} did yield statistically significant destabilization. Addition of 4000 μM Zn^{2+} was required to destabilize β2m by 14 kJ/mol. Clearly, non-native states of β2m show a strong preference for the binding of Cu^{2+} over Zn^{2+} and Ni^{2+}, suggesting well-defined positioning of the coordinating histidine side chains in these non-native states.

Native State Binding of Divalent Metal Ion. The binding constant of each mutant construct to Cu^{2+} was determined by changes in intrinsic fluorescence (*13*). H13F, H51F, and H84A have dissociation constants between 1 and 3 μM (Figure 6 and Table 1) which are comparable to WT. H31F, however, binds Cu^{2+} >10-fold weaker than the wild type with a dissociation constant of 41.0 ± 2.7 μM (Figure 6A,B). This clearly implicates H31 as the primary ligand in Cu^{2+} binding by the native conformation of β2m. As binding of Cu^{2+} to the H31F construct is not eliminated, it is likely that other residues in the vicinity of H31 also participate in forming the binding pocket (Figure 2B).

The binding constant of WT β2m to Ni^{2+} and Zn^{2+} was also determined by changes in intrinsic fluorescence. Ni^{2+} and Zn^{2+} bind much more weakly to β2m than Cu^{2+} (Figure 6C,D). As Ni^{2+} is also a fluorescence quencher, its level of binding could be determined in the same manner as that of Cu^{2+}. This yields a K_d of 400 μM (Figure 6C), more than 100-fold weaker than the interaction of Cu^{2+} with β2m. In

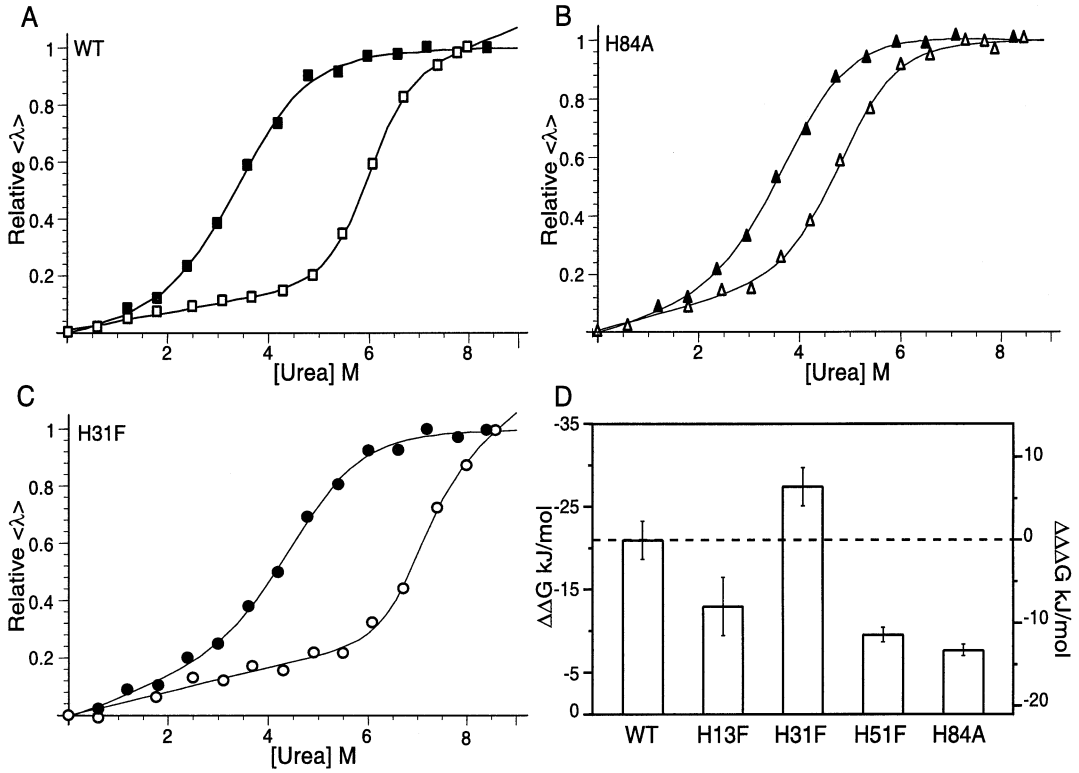

FIGURE 4: Chemical stability of β2m and mutant variants measured by changes in intrinsic fluorescence. Urea denaturation of 2.5 μM WT (A), H84A (B), and H31F (C) in the presence (filled symbols) and absence (empty symbols) of 90 μM Cu^{2+}. All denaturation data were fit to a two-state model (*25*). (D) Summary of these results for all mutants expressed on the left axis as ΔG of folding in the presence of Cu^{2+} − ΔG of folding in the absence of Cu^{2+}. To illustrate the relative increase in sensitivity of H31F to copper, and the relative decrease in sensitivity of all other mutants to copper, a labeled axis on the same scale is shown on the right but expressed relative to WT. A dotted line is drawn at the zero of the right-hand axis. Error bars are ±1 standard error of the mean (SEM).

addition, the loss of fluorescence intensity upon Ni^{2+} binding is less than that observed for Cu^{2+} (only 20% compared to 40%). This disparity could be due to the different intrinsic quenching efficiencies of the two metals. Another factor, however, could be the geometry of coordinating moieties in the binding site. These could place Ni^{2+} in a different position with respect to W60, leading to a decreased level of quenching. Since Zn^{2+} is not a quencher, its binding constant to β2m was determined by competition for the Cu^{2+} binding site by Zn^{2+} over a series of Cu^{2+} binding assays at seven different Zn^{2+} concentrations ranging from 0 to 6000 μM Zn^{2+} (Figure 6D). The binding constant of Zn^{2+} to β2m was determined by global analysis to be 1.5 mM, 500-fold above the binding constant for Cu^{2+}. Clearly, the metal binding site of native β2m is highly specific for Cu^{2+}.

Metal Binding by Native State Mass Spectrometry. Direct assessment of metal binding to β2m was made using native state electrospray ionization mass spectrometry (*26*). An electrospray mass spectrum of β2m in the presence of Cu^{2+} contains a series of peaks corresponding to β2m·$(Cu^{2+})_k$ (for $k = 0, 1, 2, ...$). Measurement of dissociation constants by mass spectrometry is complicated by the absence of a 1:1 correspondence between the measured intensity and solution concentration. Furthermore, the necessary presence of weak volatile chelates (e.g., NH_3) complicates determination of the free divalent ion concentration. We have therefore combined hWT protein with expressed proteins to allow for internal control of these factors (Figure 7A). As the recombinant constructs all contain an additional N-terminal methionine, they have an increased mass (e.g., 131 Da for rWT-hWT) which permits their resolution from hWT in

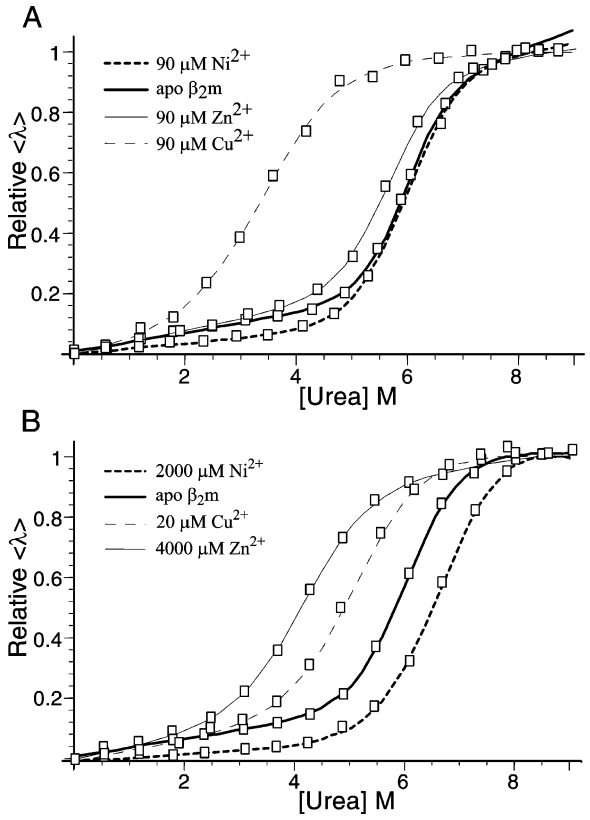

FIGURE 5: (A) Chemical stability of 2.5 μM WT β2m measured by changes in intrinsic fluorescence as a function of added urea in the absence or presence of 90 μM Cu^{2+}, Ni^{2+}, or Zn^{2+}. (B) Chemical stability in the absence or presence of 20 μM Cu^{2+}, 2000 μM Ni^{2+}, or 4000 μM Zn^{2+}.

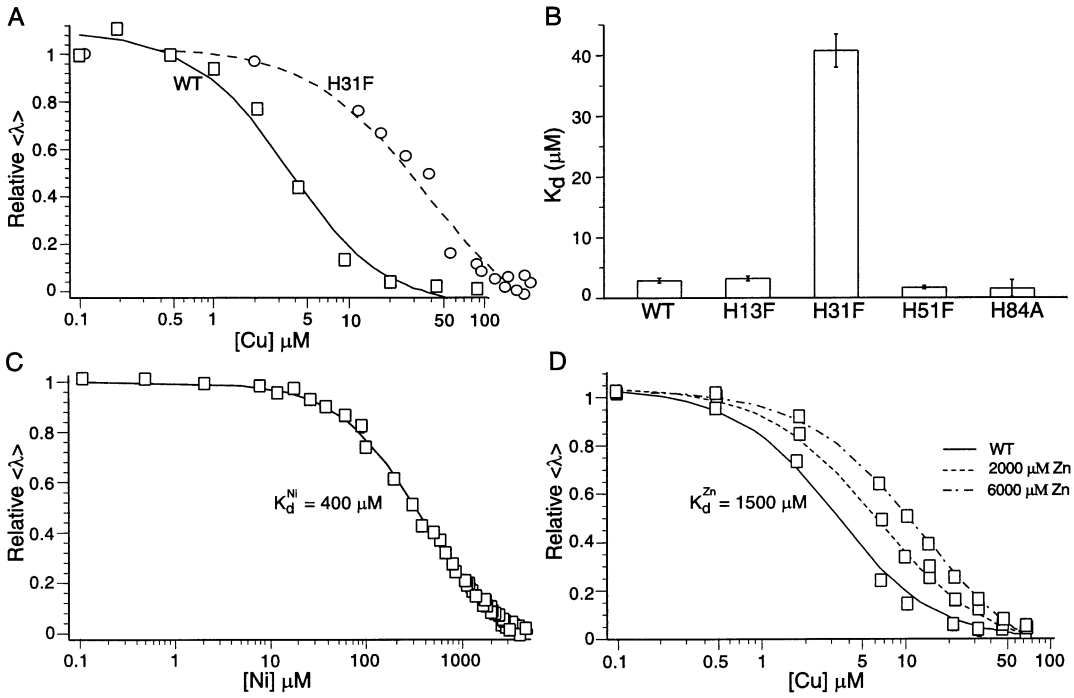

FIGURE 6: Measurement of the divalent ion affinity of mutant β2m for the folded state by changes in intrinsic fluorescence. (A) Representative plots of copper titration of WT (□) and H31F (○) are shown with nonlinear fits of equilibrium dissociation with a 1:1 stoichiometry. (B) Summary of Cu^{2+} dissociation constants measured for each construct shown with error bars at ±1 SEM. (C) Assessment of Ni^{2+} binding by titration. A nonlinear fit is shown giving a K_d of 400 μM. (D) Multiple copper titrations of β2m at seven different concentrations of Zn^{2+} were performed. Three representative data sets with fits are shown. Global fit to all the data yield a K_d for Zn^{2+} of 1500 μM.

heterogeneous mixtures. Comparisons of other closely related protein pairs suggest that it is reasonable to assume that instrument response will affect hWT·$(Cu^{2+})_k$ and rWT·$(Cu^{2+})_k$ equally for a given k within a given charge state in the same spectrum (*27*). Relative dissociation constants can therefore be accurately determined as

$$K_{d,r\beta2m}/K_{d,h\beta2m} = [r\beta2m\cdot(Cu^{2+})_0 \times h\beta2m\cdot(Cu^{2+})_1]/[h\beta2m\cdot(Cu^{2+})_0 \times r\beta2m\cdot(Cu^{2+})_1] \quad (1)$$

where each rβ2m·$(Cu^{2+})_k$ is the peak intensity from a given recombinant β2m, with k Cu^{2+} ions bound.

The Cu^{2+} binding behavior of hWT and that of rWT are indistinguishable (Figure 7A,B). At 40 μM protein and 120 μM Cu^{2+}, the dominant peak is β2m·$(Cu^{2+})_1$. A small percentage (13%) of protein can be seen binding a second Cu^{2+}. In a control experiment using hen lysozyme under matched solution conditions, a single Cu^{2+} is seen, accounting for 11% of the protein (data not shown). Since hen lysozyme is not a Cu^{2+} binding protein, this suggests that the small population of β2m with two Cu^{2+} ions is a reflection of nonspecific adduct formation resulting from the ionization process. The peak corresponding to β2m·$(Cu^{2+})_1$ includes contributions from both specific binding and nonspecific adduct formation. The contributions of the latter may be estimated by looking to the peak corresponding to β2m·$(Cu^{2+})_2$. For rWT, this peak is 20% of the height of the peak at β2m·$(Cu^{2+})_1$. The same relative proportion applied to β2m·$(Cu^{2+})_0$ indicates that only 5% of the peak at β2m·$(Cu^{2+})_1$ is due to nonspecific adduct formation. The relative K_d (eq 1) for rWT and hWT is 1.2, indicating that recombinant and human-derived protein are quantitatively as well as qualitatively identical.

Copper binding measurements of β2m constructs were conducted by mixing hWT with H13F, H31F, H51F (MW = 11 870 Da), or H84A (MW = 11 794 Da). Only H31F reveals behavior clearly distinct from that of the wild-type protein (Figure 7D). A total of 90% of hWT is in Cu^{2+}-bound states (k = 1 or 2). In contrast, 30% of H31F shows addition of only one Cu^{2+} ion. This is only slightly larger than expected for nonspecific adduct formation. Supporting this is a Cu^{2+} titration of H31F in which we observe that binding of one Cu^{2+} by H31F parallels binding of a second Cu^{2+} by hWT (data not shown). Using eq 1, we can conclude that the relative K_d of H31F for copper is minimally 13-fold greater than that of hWT. A more accurate measurement cannot be made as this is at the limit of interference from nonspecific adduct formation. The H13F and H51F mutants each bind copper with qualitative behavior which is indistinguishable from that of the hWT protein (Figure 7C). The relative dissociation constants measured using eq 1 are 1.1 and 0.5, respectively. These compare well with the values of 1.1 and 0.6 calculated from the ratio of dissociation constants obtained by fluorescence (Figure 6B). The relative K_d of H84A could not readily be determined by this approach since hWT·$(Cu^{2+})_2$ and H84A·$(Cu^{2+})_0$ are partially overlapping. Overall, we conclude that direct assessment of Cu^{2+} binding agrees with our fluorescence studies, indicating that H31 is the primary location for native state Cu^{2+} binding (Figure 6).

Assessment of Ni^{2+} binding by fluorescence (Figure 6C) does not necessarily reflect binding to the Cu^{2+} binding site. Competition of Ni^{2+} for the Cu^{2+} binding site can, however, be directly observed by ESI-MS. The high concentrations of Ni^{2+} required for binding result in ESI-MS spectra which are obscured by nonspecific adduct formation intrinsic to

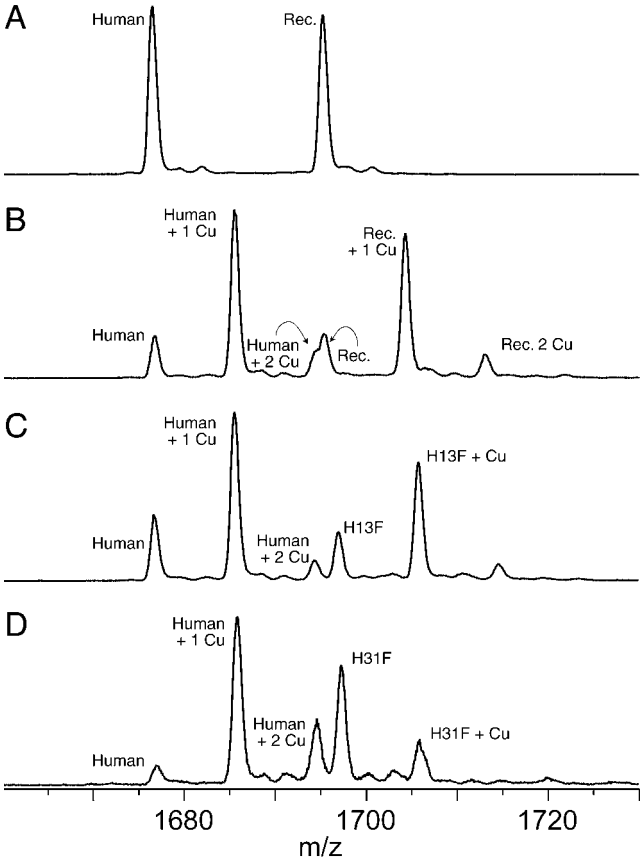

FIGURE 7: Mass spectra of folded β2m in the presence or absence of added divalent copper. To facilitate the comparison of mutant and wild-type forms of β2m, equimolar mixtures of human-derived and recombinant β2m were prepared. The total protein concentration is 40 μM. (A) Spectra of human and recombinant β2m in the absence of added metal. Only the +7 charge state is shown yielding two peaks separated by *m*/*z* 18.7. This corresponds to the additional methionine residue of recombinant β2m. (B) Human and recombinant β2m in the presence of 120 μM $CuCl_2$. (C) Human wild-type β2m and H13F in the presence of 120 μM $CuCl_2$. (D) Human wild-type β2m and H31F in the presence of 120 μM $CuCl_2$.

the electrospray process. Therefore, we have performed experiments using Ni^{2+} in the presence and absence of 60 μM Cu^{2+}. Copper binding to β2m was competed at 60 μM Cu^{2+} with 60 μM, 600 μM, and 6 mM Ni^{2+}. At a 1:1 Cu^{2+}:Ni^{2+} ratio, only Cu^{2+} binding is detected (Figure 8B). The β2m·$(metal^{2+})_1$ − β2m·$(metal^{2+})_0$ mass difference in Figure 8B is 61.3 Da which allows 94.6% of the β2m·$(metal^{2+})_1$ peak to be attributed to Cu^{2+}. At Ni^{2+} concentrations of 600 μM, the spectra become more complex due to nonspecific adduct formation (Figure 8C). Addition of 60 μM Cu^{2+} is nevertheless able to cause a significant mass shift (Figure 8D). Mass measurement of β2m·$(metal^{2+})_1$ − β2m·$(metal^{2+})_0$ peaks in Figure 8D shows that 78% of the mass shift can be attributed to Cu^{2+}. Increasing the concentration of Ni^{2+} to 6 mM gives spectra which are indistinguishable in the presence and absence of 60 μM Cu^{2+} (Figure 8E,F). Thus, we observe competition of Ni^{2+} for the Cu^{2+} binding site at a 100-fold excess of Ni^{2+}, a molar ratio comparable to the difference in the observed K_d, measured by changes in intrinsic fluorescence (Figure 6).

DISCUSSION

Elucidation of the residue specific effects of Cu^{2+} on β2m is central to understanding the mechanism of divalent induced

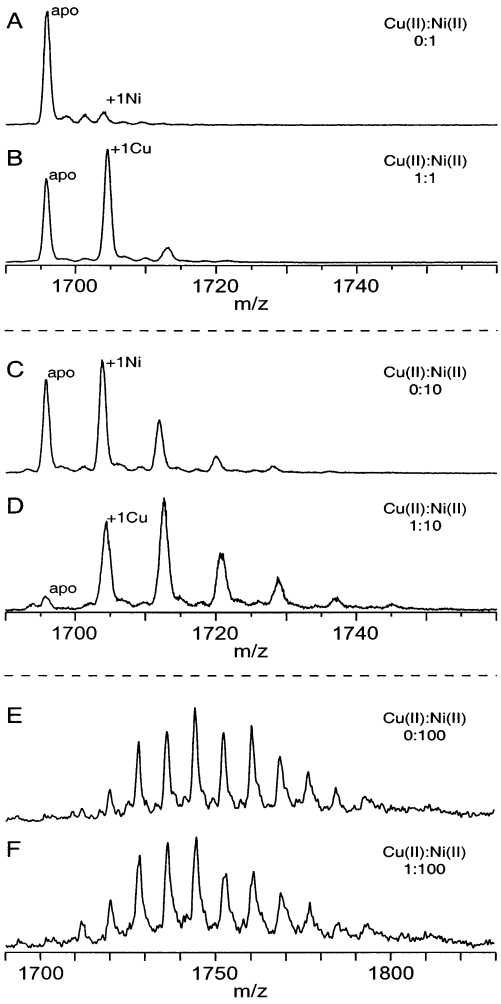

FIGURE 8: Mass spectra of rβ2m in the presence of mixtures of Cu^{2+} and Ni^{2+}. The total protein concentration is 40 μM. The Cu^{2+} concentration is 60 μM in panels B, D, and F. The Ni^{2+} concentration is 60 μM in panels A and B, 600 μM in panels C and D, and 6000 μM in panels E and F. Peaks corresponding to β2m with one associated metal are annotated with the dominant metal contributing to the mass shift. Nickel-containing spectra are dominated by ladders of peaks which correspond to nonspecific association of Ni^{2+} which occurs during the ionization process. This is most notable in panels E and F. Solution binding of Ni^{2+} to the Cu^{2+} binding site is therefore inferred from the elimination of a mass shift associated with copper binding. The copper mass shift in the presence of Ni^{2+} is most clearly evident at a 1:1 Cu^{2+}:Ni^{2+} stoichiometry (A and B). No copper mass shift is evident at a 1:100 Cu^{2+}:Ni^{2+} stoichiometry (E and F), indicating that Ni^{2+} has displaced Cu^{2+} from the binding site.

fibrillogenesis in DRA. Here we have performed a range of experiments aimed at delineating between binding and destabilization. There are four critical observations which impact our understanding of this system. (i) The native state binding site for Cu^{2+} is restricted to the vicinity of H31 and W60. (ii) Native state binding of divalent ion is specific for Cu^{2+} over Zn^{2+} and Ni^{2+}. (iii) Cu^{2+} induced destabilization of β2m is mediated by residues which are not involved in native state binding. (iv) Destabilization of β2m by divalent ions is specific for Cu^{2+} over Zn^{2+} and Ni^{2+}.

Assertions of Cu^{2+} specificity when describing metal binding by proteins are complicated by the relatively high intrinsic affinity of the imidazole group for Cu^{2+} over other metals. Ni^{2+} and Zn^{2+} are commonly used for comparison with Cu^{2+} as a result of their identical charge, and nearly

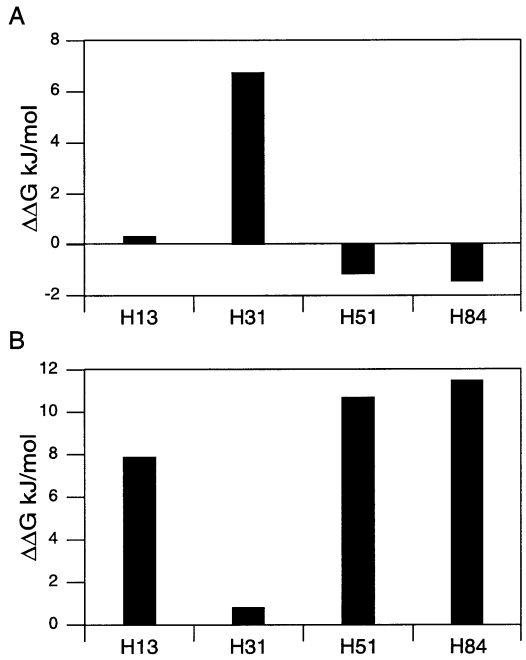

FIGURE 9: Calculated contributions of individual amino acids to the free energy of binding of Cu^{2+} to folded ($\Delta\Delta G_f^{Cu}$ = WTΔG_f^{Cu} − mutant ΔG_f^{Cu}) (A) and unfolded ($\Delta\Delta G_u^{Cu}$ from Table 1) (B) conformations of β2m. ΔG_f^{Cu} values are the free energies of copper binding at 90 μM Cu^{2+} using measured dissociation constants for each construct (Table 1, column 3).

identical ionic radii. The paradigm is that discrimination between these metals requires a well-defined three-dimensional macromolecular structure to hold coordinating ligands at fixed distances and geometry. The imidazole side chain of histidine and its related derivative 4-methylimidazole have intrinsic affinities for Cu^{2+}, Ni^{2+}, and Zn^{2+} of 63−66 μM, 0.9−1.2 mM, and 2.8−3.3 mM, respectively, in aqueous solution (*28*). This obeys the Irving−Williams series, which relates the decrease in ionic radii with stronger metal−ligand interaction. In this work, we have made comparisons of Cu^{2+} with Ni^{2+} or Zn^{2+} at 1:1 ratios, but also at ratios of approximately 1:10 and 1:100 for Cu^{2+}:Ni^{2+} and Cu^{2+}:Zn^{2+}, respectively. This permits us not only to evaluate absolute specificity of copper effects but also to characterize the relative contribution of intrinsic chemistry and macromolecular structure.

Native state β2m binds Cu^{2+} specifically with an affinity of 2.8 μM and maps via NMR (Figure 1) and mutagenesis to H31 (Figures 6 and 9A). As this binding constant is ~20-fold tighter than the intrinsic affinity of imidazole for copper, it suggests that other substituents provide energetically favorable coordination to the metal. These ligands may include the protein backbone, water, and/or W60. This would be similar to coordination of Cu^{2+} by His, Gly backbone, water, and Trp recently reported for the octapeptide repeat of mammalian prion (*29*). Competition of Cu^{2+} with Ni^{2+} in mass spectra clearly shows Ni^{2+} and Cu^{2+} bind to the same site in β2m (Figure 8). Competition of Cu^{2+} by Zn^{2+} in fluorescence spectra also shows Cu^{2+} and Zn^{2+} bind to the same site in β2m (Figure 6). The affinities of β2m for Ni^{2+} and Zn^{2+} are 400 and 1500 μM, respectively. These are ~$^1/_{100}$ and ~$^1/_{500}$ of the binding constant for Cu^{2+}, and 10- and 5-fold, respectively, less than expected for binding by an unstructured imidazole. Thus, the additional substituents which enhance copper binding not only are increasing affinity but also are structured to enhance specificity for copper. The specificity of Cu^{2+} binding to β2m is therefore the result of a defined metal binding site.

Binding of copper by β2m is favorable and therefore must stabilize the native state relative to unfolded state(s). To account for the net destabilization of β2m by metal, the unfolded state must also bind Cu^{2+}. In principle, any protein containing a buried histidine should yield this effect. Consider a hypothetical protein with a buried histidine which is wholly exposed upon unfolding. Given a dissociation constant of 4-methylimidazole for Cu^{2+} of 66 μM and a copper concentration of 90 μM, for example, in Figure 4, this gives a net destabilization of ~0.7 kJ/mol. This is small compared to the value of 20−60 kJ/mol that is typical of protein stability and is consistent with the fact that histidine residues are frequently observed within the interior of protein structures. Of the four histidine residues of β2m, only one is completely buried (H84; see Table 1). If it is assumed that all were buried and all were exposed upon unfolding to a random coil state, the net destabilization would be ~2.8 kJ/mol. This is on the order of $^1/_{10}$ of the observed $\Delta\Delta G$ upon metal binding (Figure 4D) which indicates that additional structural factors must contribute to the observed destabilization.

Analysis of structural factors relevant to destabilization of β2m is conducted here by mutation at each histidine residue. This has demonstrated that native state binding and protein destabilization are structurally distinct events. Mutation of H31 to phenylalanine increases the sensitivity of β2m to destabilization by Cu^{2+} by 5.9 kJ/mol over that of the wild type ($\Delta\Delta\Delta G$, Figure 4D). We further note that the level of native state binding to Cu^{2+} diminishes from 3 to 40 μM upon mutation of H31 (Figure 6B). This corresponds to a relative change in binding induced stability ($\Delta\Delta G$) of 6.4 kJ/mol at 90 μM Cu^{2+}. Clearly, the change in binding energy is within error of the change in copper induced destabilization. This suggests that the entirety of the increased sensitivity of H31F to unfolding by copper is due to the loss of stabilization of the native state provided by ligand binding. We initially suggested that binding of Cu^{2+} by β2m was destabilizing in a manner akin to protonation (*13*); i.e., binding and destabilization could be mediated by the same residues. Others have also offered reasonable explanations for the creation of non-native states upon copper binding by the folded protein (*23*). However, the changes in energetics observed here for H31F are at odds with these explanations. If it is assumed that amyloidosis in β2m requires destabilization of the folded state to populate amyloidogenic intermediates, then the structures formed upon native state binding of Cu^{2+} (Figure 2B) are unlikely to represent such an intermediate.

Histidine residues 13, 51, and 84 all contribute to the destabilization of β2m. The simplest model in which to interpret these results is

$$UCu_n \overset{K_d^U}{\longleftrightarrow} U + nCu \overset{K_u}{\longleftrightarrow} F + Cu \overset{K_d^F}{\longleftrightarrow} FCu$$

Separate dissociation constants describe binding to either the unfolded state (K_d^U) or the folded state (K_d^F). The folding stability is characterized by K_u and is invariant to changes

in copper concentration. n is the stoichiometry of this binding and has two limiting conditions: $n = 1$, which requires cooperative formation of a binding site in which all three histidine residues participate in the coordination of metal, and $n = 3$, in which each histidine binds independently to a separate Cu^{2+}.

In the context of this model, the changes in stability due to copper (Figure 4) are solely the result of metal binding to the unfolded state. The $\Delta\Delta G_u^{Cu}$ values for the contribution of each histidine to the destabilization of β2m (Figure 9B and Table 1) confirm that H31 does not participate in protein destabilization. Whereas H13, H51, and H84 each contribute on the order of 10 kJ/mol to the destabilization of the protein, H31 gives less than 1 kJ/mol. The sum of the free energies of H13, H51, and H84 mutants is 30.7 kJ/mol which is within 1.1 kJ/mol of the destabilization of the wild-type protein (29.6 kJ/mol, Table 1). This suggests that all of the destabilization is additive and mediated by these three histidine residues.

Destabilization is most likely mediated by the coordination of a single ($n = 1$) copper by H13, H51, and H84. The magnitude of the free energy contribution of each histidine (H13, H51, and H84) to destabilization each exceeds by greater than a factor of 10 the magnitude we calculate from changes in solvent exposure of a buried histidine (0.7 kJ/mol; see above). In addition, since H13 and H51 are mostly exposed (~70%) even in the folded state, there is an even narrower scope for single coordination of copper by individual histidine residues to contribute to the destabilization of this protein. Recent work has indicated a possible role for a number of residues, including H84, as being central to the formation of an acid molten globule state of β2m (*30*). H84A is the least sensitive of our constructs to destabilization by Cu^{2+}. It is possible, therefore, that acid molten globular structures are similar to copper induced conformational states.

The most compelling reason to assert the existence of a single copper center in non-native β2m is the observation of specificity for Cu^{2+} over Ni^{2+} and Zn^{2+} for destabilization. When the stabilization of the native protein by metal ion binding is taken into account (see the above model), Cu^{2+} binding to the unfolded state contributes 17.1 kJ/mol at 20 μM Cu^{2+} while Zn^{2+} contributes 18.4 kJ/mol at 4000 μM. At 2000 μM Ni^{2+}, the contribution of binding to the unfolded state is 8.2 kJ/mol. Binding to the native state accounts for all observed effects due to Ni^{2+}. The requirement for nearly 1000-fold greater Zn^{2+} than Cu^{2+} for an equivalent energy of binding to the unfolded state is consistent with changes in the affinity of three imidizole groups for these metals (*28*); i.e., the selectivity of Cu^{2+} over Zn^{2+} by the unfolded state is largely derived from differences in the intrinsic affinity of imidazole for these two metals. However, intrinsic affinities of three coordinating imidazoles are nearly identical for Zn^{2+} and Ni^{2+}. The absence of any apparent binding by Ni^{2+} to the unfolded state of β2m requires that we invoke protein structure to account for the selectivity. We conjecture that the nature of this structure is tetrahedral as Cu^{2+} and Zn^{2+} prefer this binding geometry. Ni^{2+}, in contrast, prefers a square planer arrangement of its ligands.

The presence of a well-defined substructure in non-native, unfolded states of β2m is exciting given our recent evidence suggesting Cu^{2+} is central to amyloid formation and pathogenesis of DRA (*13*). Destabilization of protein native structure is generally a prerequisite for fibrillogenesis (*31*). However, wholly unfolded states of amyloid proteins, e.g., transthyretin, are not thought to contribute greatly to assembly. While specific formation by unfolded states seems to be implausible, it has recently been observed that local structure exists in unfolded states of several model systems, e.g., reduced lysozyme (*32*) and staphylococcal nuclease (*33*). Some amyloid proteins may therefore have sequences which, in the presence of divalent cation, give rise to well-defined substructures within an otherwise unfolded polypeptide chain. It is these structures that may then contribute to amyloid assembly. As Cu^{2+} has been recently implicated in Alzheimer's (*10*), Parkinson's (*11*), prion protein (*9*), and immunoglobulin light chain amyloidosis (*12*), the generality of this phenomenon may prove to be widespread.

ACKNOWLEDGMENT

We thank Dr. A. Valentine and Dr. S. Jaswal for helpful suggestions and critical reading of the manuscript. We thank Dr. E. M. De La Cruz for help with data analysis. We thank Dr. G. Sarkis for assistance with molecular biology. We thank Prof. L. Regan for use of the CD spectrophotometer.

REFERENCES

1. Rochet, J. C., and Lansbury, P. T., Jr. (2000) *Curr. Opin. Struct. Biol. 10*, 60−68.
2. Fandrich, M., Fletcher, M. A., and Dobson, C. M. (2001) *Nature 410*, 165−166.
3. Sunde, M., Serpell, L. C., Bartlam, M., Fraser, P. E., Pepys, M. B., and Blake, C. C. (1997) *J. Mol. Biol. 273*, 729−739.
4. Harper, J. D., and Lansbury, P. T., Jr. (1997) *Annu. Rev. Biochem. 66*, 385−407.
5. Chien, P., and Weissman, J. S. (2001) *Nature 410*, 223−227.
6. Scherzinger, E., Sittler, A., Schweiger, K., Heiser, V., Lurz, R., Hasenbank, R., Bates, G. P., Lehrach, H., and Wanker, E. E. (1999) *Proc. Natl. Acad. Sci. U.S.A. 96*, 4604−4609.
7. Osherovich, L. Z., and Weissman, J. S. (2001) *Cell 106*, 183−194.
8. Perutz, M. F., Johnson, T., Suzuki, M., and Finch, J. T. (1994) *Proc. Natl. Acad. Sci. U.S.A. 91*, 5355−5358.
9. Jobling, M. F., Huang, X., Stewart, L. R., Barnham, K. J., Curtain, C., Volitakis, I., Perugini, M., White, A. R., Cherny, R. A., Masters, C. L., Barrow, C. J., Collins, S. J., Bush, A. I., and Cappai, R. (2001) *Biochemistry 40*, 8073−8084.
10. Miura, T., Suzuki, K., Kohata, N., and Takeuchi, H. (2000) *Biochemistry 39*, 7024−7031.
11. Uversky, V. N., Li, J., and Fink, A. L. (2001) *J. Biol. Chem. 276*, 44284−44296.
12. Davis, D. P., Gallo, G., Vogen, S. M., Dul, J. L., Sciarretta, K. L., Kumar, A., Raffen, R., Stevens, F. J., and Argon, Y. (2001) *J. Mol. Biol. 313*, 1021−1034.
13. Morgan, C. J., Gelfand, M., Atreya, C., and Miranker, A. D. (2001) *J. Mol. Biol. 309*, 339−345.
14. Bjorkman, P. J., Saper, M. A., Samraoui, B., Bennett, W. S., Strominger, J. L., and Wiley, D. C. (1987) *Nature 329*, 506−512.
15. Floege, J., and Ehlerding, G. (1996) *Nephron 72*, 9−26.
16. Okon, M., Bray, P., and Vucelic, D. (1992) *Biochemistry 31*, 8906−8915.
17. Royer, C. A., Mann, C. J., and Matthews, C. R. (1993) *Protein Sci. 2*, 1844−1852.
18. Pearson, W. R. (1990) *Methods Enzymol. 183*, 63−98.
19. Brown, N. P., Leroy, C., and Sander, C. (1998) *Bioinformatics 14*, 380−381.
20. Koradi, R., Billeter, M., and Wuthrich, K. (1996) *J. Mol. Graphics 14*, 51−55.

21. Delaglio, F., Grzesiek, S., Vuister, G. W., Zhu, G., Pfeifer, J., and Bax, A. (1995) *J Biomol NMR 6*, 277−293.
22. Goddard, T. D., and Kneller, D. G. (2002) *Sparky*, University of California, San Francisco.
23. Verdone, G., Corazza, A., Viglino, P., Pettirossi, F., Giorgetti, S., Mangione, P., Andreola, A., Stoppini, M., Bellotti, V., and Esposito, G. (2002) *Protein Sci. 11*, 487−499.
24. Collins, E. J., Garboczi, D. N., and Wiley, D. C. (1994) *Nature 371*, 626−629.
25. Bolen, D. W., and Santoro, M. M. (1988) *Biochemistry 27*, 8069−8074.
26. Miranker, A. D. (2000) *Curr. Opin. Struct. Biol. 10*, 601−606.
27. Larson, J. L., Ko, E., and Miranker, A. D. (2000) *Protein Sci. 9*, 427−431.
28. Smith, R. M., and Martell, A. E., Eds. (1989) *Critical Stability Constants*, Plenum Press, New York.
29. Burns, C. S., Aronoff-Spencer, E., Dunham, C. M., Lario, P., Avdievich, N. I., Antholine, W. E., Olmstead, M. M., Vrielink, A., Gerfen, G. J., Peisach, J., Scott, W. G., and Millhauser, G. L. (2002) *Biochemistry 41*, 3991−4001.
30. McParland, V. J., Kad, N. M., Kalverda, A. P., Brown, A., Kirwin-Jones, P., Hunter, M. G., Sunde, M., and Radford, S. E. (2000) *Biochemistry 39*, 8735−8746.
31. Kelly, J. W. (1998) *Curr. Opin. Struct. Biol. 8*, 101−106.
32. Klein-Seetharaman, J., Oikawa, M., Grimshaw, S. B., Wirmer, J., Duchardt, E., Ueda, T., Imoto, T., Smith, L. J., Dobson, C. M., and Schwalbe, H. (2002) *Science 295*, 1719−1722.
33. Shortle, D., and Ackerman, M. S. (2001) *Science 293*, 487−489.
34. Koradi, R., Billeter, M., and Wuthrich, K. (1996) *J. Mol. Graphics 14*, 29−32.

BI025944A